Effects of Synthesis on the Structural Properties and Methane Partial Oxidation Activity of Ni/CeO$_2$ Catalyst

Valeria La Parola [ID], **Giuseppe Pantaleo and Anna Maria Venezia** * [ID]

Istituto per lo Studio dei Materiali Nanostrutturati (ISMN-CNR), Via Ugo la Malfa 153, 90146 Palermo, Italy; laparola@pa.ismn.cnr.it (V.L.P.); pantaleo@pa.ismn.cnr.it (G.P.)
* Correspondence: annamaria.venezia@cnr.it; Tel.: +39-091-680-9372

check for
updates

Abstract: Nickel catalysts supported on homemade CeO$_2$ oxide were prepared by two procedures intending to achieve different degree of metal-support interaction. One method consisted of a co-precipitation that was assisted by microwave; the other method was based on a modified wetness impregnation in the presence of the organic complexing ligand, nitrilotriacetic acid (NTA). The support and catalysts were characterized by temperature programmed reduction (TPR), X-ray diffraction (XRD), and X-ray photoelectron spectroscopy (XPS) techniques. Significant differences in the structure, in redox properties and in the elemental surface composition emerged. The catalytic behavior in the partial oxidation of methane was tested at atmospheric pressure, in a range of temperature between 400–800 °C, using diluted feed gas mixture with CH$_4$/O$_2$ = 2 and GHSV = 60,000 mL g^{-1} h^{-1}. Moreover, the effect of the catalyst reduction pretreatment was investigated. The better catalytic performance of the microwave-assisted sample as compared to the NTA prepared sample was attributed to the stronger interaction of nickel with CeO$_2$. Indeed, according to the structural and reducibility results, an adequate electronic contact between the metal and the support favors the formation of oxygen vacancies of ceria and inhibits the sintering of the catalyst active species, with an improvement of the catalytic performance.

Keywords: NiCeO$_2$ catalysts; catalytic partial oxidation (CPO); Methane; metal–support interaction

1. Introduction

The production of syn gas, a mixture of hydrogen and carbon monoxide, is a crucial process in relation to the transformation of methane to higher hydrocarbons through the Fisher–Tropsch Synthesis (FTS), or to high value chemicals or in relation to the production of hydrogen, which can be converted into electricity through fuel cell technology [1]. The main process that is used in industry for syngas generation is the steam reforming of methane (SRM). However, such a reaction is strongly endothermal and it demands lot of energy to the system. On the contrary, methane catalytic partial oxidation (CPOM) is a more energy and cost-effective method in virtue of its mild exothermicity. It allows 10–15% reduction in the energy requirement as compared to SRM. Additionally, the produced synthesis gas with H$_2$/CO = 2 is suitable for methanol and Fisher–Tropsch syntheses [2]. In terms of cost and availability, nickel is the metal of choice for such a catalytic reaction. Nevertheless, in order to avoid the drawback of an easy deactivation by carbon and metal sintering, various oxide supports were investigated [3–6]. When oxidation processes are involved, CeO$_2$, in virtue of its peculiar redox properties, is a particularly good catalyst carrier [7–10]. Several studies have confirmed the importance of the CeO$_2$ morphology on the supported nickel catalysts for different types of reaction, from the CO and propane oxidation to the steam reforming of methane [11–13]. These studies have shown a close relationship between the ceria morphology and the nickel–support interaction.

　　　　Related to the experimental conditions of the reaction, two mechanisms for the partial oxidation of methane have been proposed, the direct partial oxidation route and the combustion- reforming reaction mechanism [2,14]. The direct mechanism, which is preferentially occurring at very short time (~10^{-3} s), involves the dissociation of methane to carbon and hydrogen, with carbon reacting with oxygen, forming CO, and the hydrogen desorbing as H_2. The so-called "combustion-reforming mechanism" involves highly exothermic combustion of methane, followed by the endothermic reforming reactions of the remaining methane with carbon dioxide and water, leading to CO and H_2. In both cases, the role of oxygen is important, and, according to the Mars van Krevelen mechanism, an enhanced mobility of the CeO_2 oxide structural oxygen contributes to the reaction of carbon to form CO [15]. The interaction between the metal and support, occurring at the metal–oxide interface contributes to the enhanced oxygen mobility [11]. Moreover, as recently demonstrated for the partial oxidation of methane, the behavior of CeO_2 supported nickel catalyst is highly dependent on the catalyst preparation procedure. Irrespective of identical chemical formulation, differences in the catalyst activity and stability were observed [16,17]. However, contrary to the above literature, describing how different preparation procedures attained different support morphology, the approach of the present investigation was to use different types of synthesis to tune the nickel-support interaction. To this aim, two different methods for anchoring the nickel to the CeO_2 support were selected. The two methods, one using microwave and the other using a metal chelating agent, afforded catalysts with a different degree of metal-support interaction. Structural and electronic properties of the obtained catalysts were investigated by X-ray diffraction (XRD), temperature programmed reduction (TPR), and thermogravimetric analyses (TGA) techniques. The effect of the structural differences was evaluated in CH_4 partial oxidation reaction. Variations in the catalytic behavior are discussed in terms of the nickel–CeO_2 interaction.

2. Results and Discussion

2.1. Catalytic Activity

　　　　In Figure 1, the catalytic behavior of the two Ni catalysts is displayed as a function of reaction temperature and time on stream. In order to investigate the effect of the catalyst pretreatment, the activities obtained with the oxidized samples and the activities of the pre-reduced samples are compared. The two catalysts behaved quite differently either when they were simply pre-oxidized or when they were pre-reduced in hydrogen flow.

　　　　The microwave activated catalyst, Ni/CeO_2*mw* without pre-reduction, has a methane conversion of 74% already at 550 °C with 60% of CO selectivity. Moreover, after reaching 90% methane conversion and 85% CO selectivity at 750 °C, during the descending temperature, the catalyst slightly deactivated. Then, it reached a stable methane conversion of 50% at 600 °C for the monitored time of 15 h. As expected, when total oxidation to CO_2 is also taking place, the molar ratio between H_2 and CO turns out to be above the stoichiometric value of 2, which is typical of the methane partial oxidation outcome. The occurrence of steam reforming may contribute to the increase of the hydrogen production. In accord with what was observed previously on Ni catalysts that were supported on CeO_2-La_2O_3 mixed oxide, the pre-treatment in hydrogen does not significantly affect the catalytic activity of this sample [18]. Different behavior is seen with Ni/CeO_2*NTA* catalyst, depending on whether it is just oxidized or pre-reduced. When this sample is tested without being pre-reduced, methane conversion of 92% and CO selectivity of 83% are obtained at the lower temperature of 650 °C. Thereafter, during the temperature increase up to 800 °C, a drastic deactivation is occurring. The deactivation continues through the descending temperature, reaching at 600 °C 20% of methane conversion totally leading to the complete oxidation to CO_2. Moreover, after the pre-treatment in hydrogen, the catalyst is completely inactive in partial oxidation of methane, exhibiting only a maximum of 30% conversion to CO_2 at 800 °C.
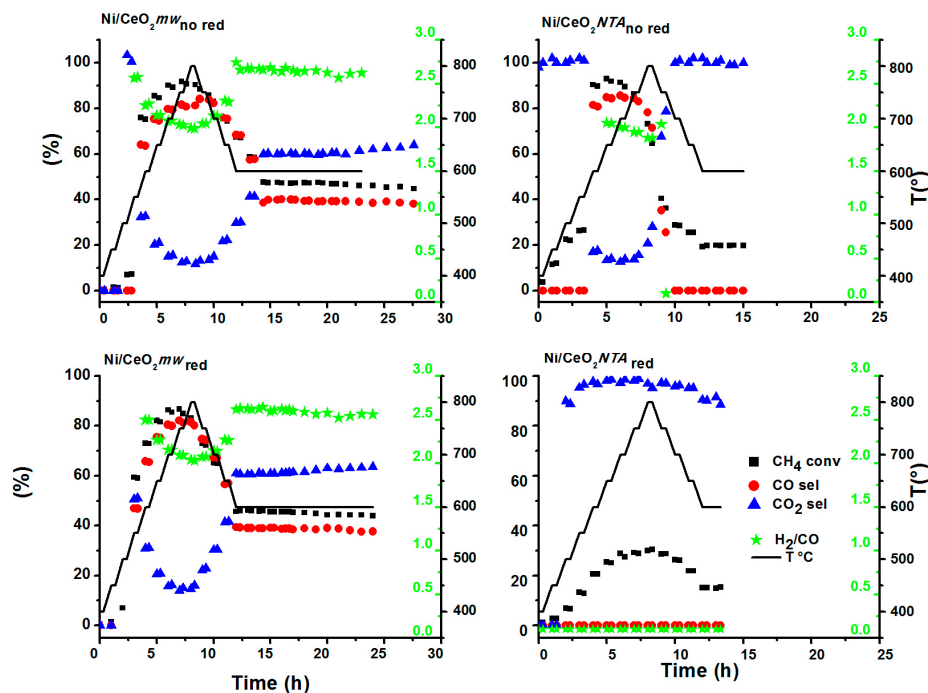
Figure 1. Influence of temperature and time on stream on CH_4 conversion and CO, CO_2 selectivities, and H_2/CO ratio.

In order to check for the presence of carbon, TGA analyses were performed on the samples after the CPO reaction. The obtained profiles, which are shown in Figure 2, indicate that no carbon accumulated over the catalyst during the period of reaction. Interestingly, from the structural point of view, opposite to the NTA sample, some weight gain is registered for the microwave sample, which is attributable to sample oxidation, either due to cerium(III) and/or Ni^0, by the air during the TG analysis.
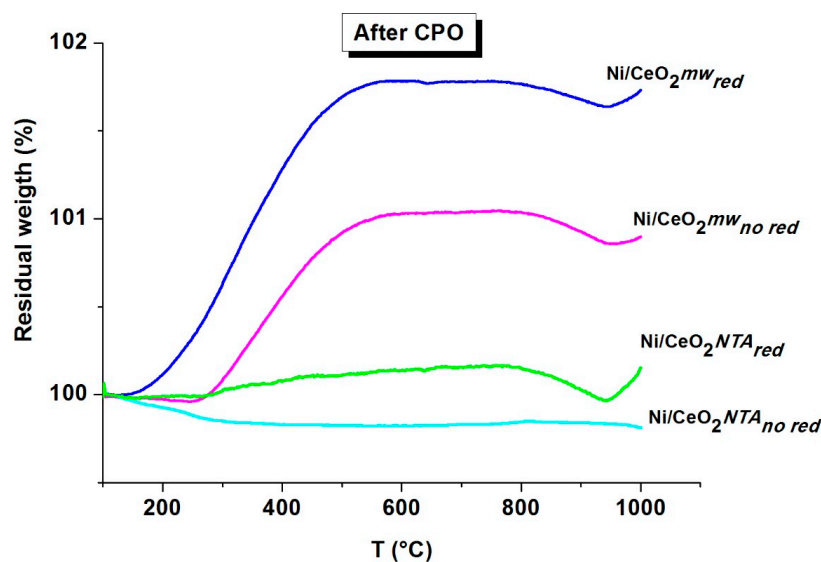

Figure 2. Thermogravimetric analyses (TGA) profiles of nickel catalyst after methane catalytic partial oxidation (CPOM) test.

The slight variations (<0.1%) of the residual weight observed at ~950 °C may correspond to some structural modification, which, given the high temperature, is not at this moment relevant for the present discussion.

To investigate the activation of methane by the catalyst, temperature programmed surface reaction with methane (CH_4-TPSR) was monitored. The desorption profiles of the reagent and product molecules arising from the reaction, CH_4, H_2, and CO, are plotted in Figure 3 for the two catalysts. Obviously, the Ni/CeO$_2$*NTA* is decomposing methane in quite larger amount when compared to the Ni/CeO$_2$*mw* catalyst. The Ni/CeO$_2$*mw* sample presents a small decomposition peak at 620 °C, corresponding to about 13% methane decomposition. On the contrary, the Ni/CeO$_2$*NTA* has a large peak at 750 °C, corresponding to 77% methane decomposition. In both cases, stoichiometric amounts of hydrogen evolved. For these samples, the volume of evolved CO_2 was negligible. However, it is worth to compare the amount of CO that was formed with the two catalysts. Indeed, if one considers the integrated ppm of CO relative to the ppm of converted methane, the ratios are 22% for the Ni/CeO$_2$*NTA* against 52% for the NiCeO$_2$*mw*. The oxygen released in CO must come, for the most part, from the CeO$_2$. Therefore, the amount of evolved CO could be considered a good indication of the oxygen mobility of the ceria support [11].
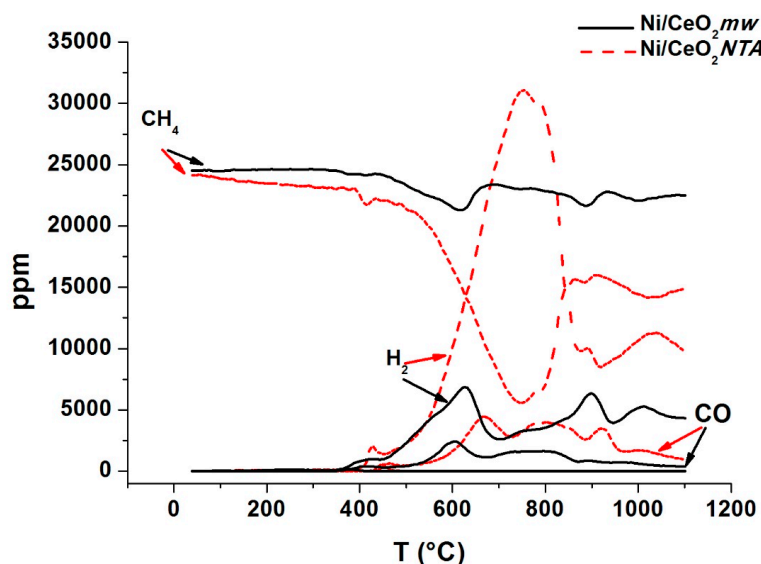

Figure 3. Temperature programmed surface reaction with methane (CH_4-TPSR) over the two different nickel catalysts pre-reduced in H_2.

Since the CeO$_2$ oxides of the two samples are similar, as confirmed by the structural and morphological data in Table 1, the reason for the different oxygen mobility could be ascribed to the method of nickel anchoring affecting the contact between Ni and CeO$_2$ [19].

Table 1. Specific surface area (BET), NiO, and CeO$_2$ crystallite sizes (d) [a] and CeO$_2$ lattice parameter (a) [b].

Sample		BET (m^2/g)	NiO d (nm)			CeO$_2$ d (nm)			Lattice Parameter a (Å)
			Fresh	Aged		Fresh	Aged		Fresh CeO$_2$
				No Red	Red		No Red	Red	
Support	CeO$_2$	30	-	-	-	18	-	-	5.411
Catalyst	Ni/CeO$_2$*mw*	26	nd	nd	nd	13	15	17	5.412
	Ni/CeO$_2$*NTA*	28	13	49	60	16	30	34	5.410

[a] Sizes are obtained from X-ray diffraction (XRD) peak line broadening according to the Scherrer analyses;
[b] Calculated from the strongest CeO$_2$(111) reflection through the equation a = (h^2 + k^2 + l^2)$^{1/2}$ (λ/2 sin ϑ) [20].

Moreover, to explain the different catalytic behavior that was observed between the unreduced and the pre-reduced Ni/CeO$_2$*NTA* sample, the CH$_4$-TPSR test was also performed on the oxidized catalyst, Ni/CeO$_2$*NTA*$_{no\ red}$. The two profiles for the reduced and unreduced sample are compared in Figure 4.

The temperature when the unreduced sample starts converting methane in significant amount is about 100 °C lower than for the reduced sample, and, overall, more methane is decomposed within the 500–900 °C temperature range. Accordingly, a larger amount of stoichiometric hydrogen evolved, whereas a more or less similar quantity of CO, from the reduced and un-reduced sample, formed. Moreover, in the profile of the unreduced sample, a small but still sizable amount of CO$_2$ was detected. The described discrepancies may be related with the fact that, in the unreduced sample, methane first is reducing the NiO, accompanied by some CO$_2$ evolution, and then it decomposes over the metallic nickel. Assuming that such a process is occurring during the CPO reaction of the unreduced Ni/CeO$_2$*NTA* sample, the generation of metallic nickel by reduction with CH$_4$, that is present in the feeding gas, accounts for the CPO activity, as observed in Figure 1, up to 600 °C. Above this temperature, the sintering of Ni particles is likely a consequence of the lack of interaction with the support. Therefore, the deactivation of the catalyst, undergoing an easier oxidation by the available oxygen in the feed, follows. The carbon deposition after CH$_4$-TPSR was checked by TGA analyses. As shown in Figure 5, the NTA samples, reduced and unreduced, exhibit weight loss corresponding to the burned off carbon. On the contrary, no weight loss is registered from the microwave sample, which was tested only after being reduced.
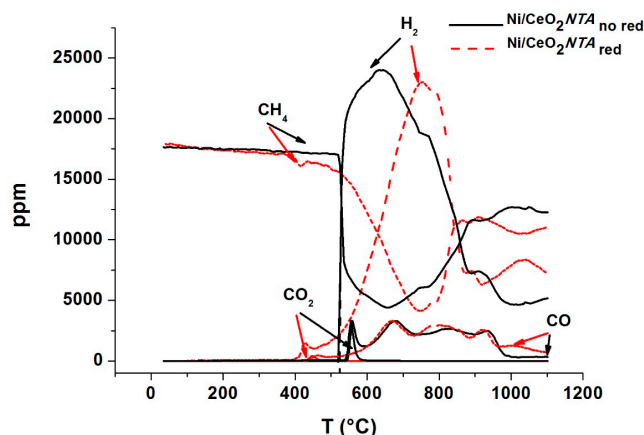

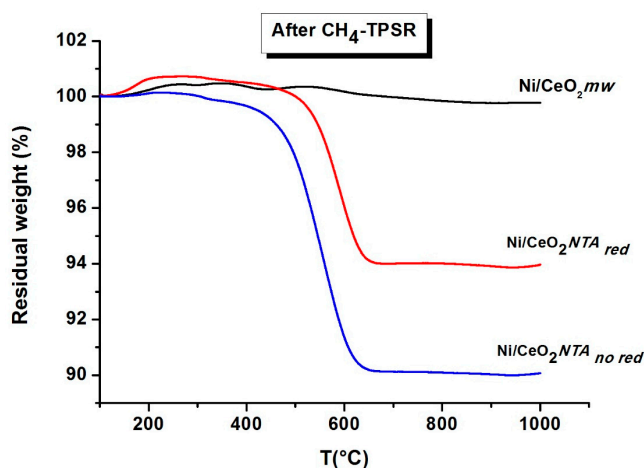**Figure 4.** Comparison of CH$_4$-TPSR over NiCeO$_2$*NTA* after different pre-treatment.

Figure 5. TGA profiles of nickel catalyst after methane CH$_4$-TPSR test.

These TGA profiles are in accord with the differences, as discussed above, in the relative CO evolution during the CH$_4$-TPSR. In other words, the nickel perturbed by the interaction with ceria is able to dissociate methane. The support, with an enhanced oxygen mobility, avoids the carbon buildup on the catalyst surface.

2.2. Characterization

The X-ray excited photoelectron region, including the experimental Ni 2p and Ce 3d photoelectron spectra, along with the fitted peaks, is shown in Figure 6. The spectra refer to the samples in the oxidized (fresh) state, and to the samples after CPO reaction.
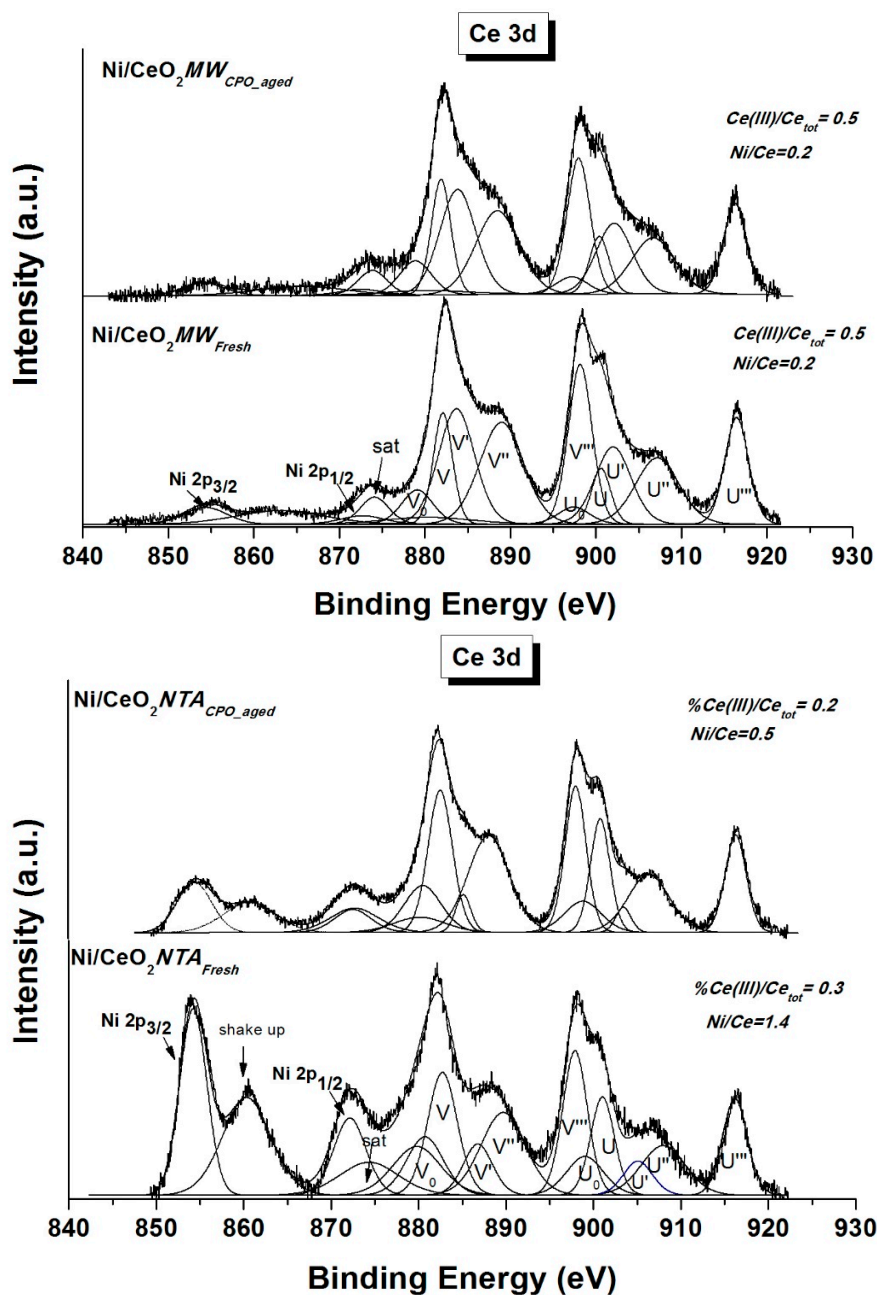

Figure 6. Ni 2p and Ce 3d photoelectron spectra of the catalysts as fresh and after the catalytic partial oxidation (CPO) test.

The spin orbit components of Ni 2p with shake up features 6 eV above the binding energy of the main peaks, which are typical of Ni(II), are present in both fresh samples. The binding energy of Ni $2p_{3/2}$, which is located at around 854–855 eV, is characteristic of NiO and Ni(OH)$_2$ [21]. The binding energy positions of the peaks do not change upon catalytic reaction. The Ce 3d spectra are rather complex, due to multiplet splittings of the final states. All of the possible electronic states arising from Ce(III) and Ce(IV) ions are labeled according to the established notation [22,23]. Curve fitting allowed for identifying ten peaks, six of which arising from Ce(IV$^)$ species and four from Ce(III) species. The two sets of spin-orbit multiplets, corresponding to the $3d_{3/2}$ and $3d_{5/2}$ states are labeled as U and V respectively. As it is well known, CeO$_2$ has a high oxygen storage capacity with high mobility of lattice and surface oxygen, which, under the X-ray exposure inside the XPS apparatus, gives rise to Ce(III) ions with the creation of oxygen vacancies, even in the calcined (fresh) samples [24,25]. In addition to the binding energy position of the peaks, curve fitting allowed for obtaining the atomic percentages of the chemical species, specifically, nickel and cerium. The atomic ratios, as given from XPS quantitative analyses, are indicated on the spectra in Figure 6. As expected from the two different preparation procedures, one based on co-precipitation of nickel and cerium species and the other based on impregnation of the complexed nickel over ceria, the corresponding atomic ratios are quite different. The Ni/Ce ratio of Ni/CeO$_2$*NTA* sample is almost three times larger than the Ni/Ce ratio of Ni/CeO$_2$*mw* sample and larger than the analytical ratio. Since the analytical composition was the same for both, it is evident the larger surface segregation of nickel on the former sample. At the same time, the ratio Ce(III)/Ce$_{tot}$ that was obtained in the NTA sample is about half the corresponding ratio of the Ni/CeO$_2$*mw* catalyst. Since the exposure to the X-rays of the XPS measurements was roughly the same, the larger ratio reflects a larger number of oxygen vacancies, very important for the catalytic promoting effect of CeO$_2$ [19]. Moreover, it is worth noting the modification undergone by the Ni/Ce atomic ratios upon catalytic reaction. Whereas, the value is stable in Ni/CeO$_2$*mw*, it decreases by more than 60% in Ni/CeO$_2$*NTA*, The differences are attributable to the superior structural stability of the microwave prepared sample, as compared to the complexing ligand prepared sample.

In order to investigate the sample reducibility, H$_2$ TPR measurements of the two fresh samples were performed. The TPR profiles of the catalysts and bare CeO$_2$ are shown in Figure 7. The temperatures of the peaks and the corresponding volumes of the consumed hydrogen are summarized in Table 2. The support profile contains a weaker feature below 600 °C, due to the surface ceria reduction, and a strong peak at around 800 °C that was attributable to ceria bulk reduction [17]. The two catalyst profiles contain the ceria bulk peak at 800 °C and strong features between 200–600 °C of different shapes. The sample prepared by the NTA complexing route exhibits a strong peak at 343 °C and two other smaller peaks at 250 and 170 °C. The one at 343 °C is due to the reduction of small NiO particles, and those at lower temperatures are due to larger NiO particles [26]. Quite differently, the sample that was prepared by microwave-assisted co-precipitation has a broad and strong peak at 450 °C which, as previously reported for similarly prepared sample, partially overlaps with the surface ceria reduction peak [17]. The reduction of Ni(II) to Ni(0), in both samples containing 6 wt % Ni, would require 23 mL/g of H$_2$. Variations in the H$_2$ volume consumption, as observed in correspondence of the nickel related TPR peaks, suggest the contribution from Ce(IV) reduction to Ce(III). Therefore, as given in Table 2, the large hydrogen volume consumption in correspondence of the 450 °C peak in the NiCeO$_2$*mw* sample confirms indeed the mutual effect of ceria and nickel oxide on the sample reducibility. The results, illustrated in Figure 7 and in Table 2, reflect quite clearly the different degree of interaction between nickel and ceria in the two catalysts.
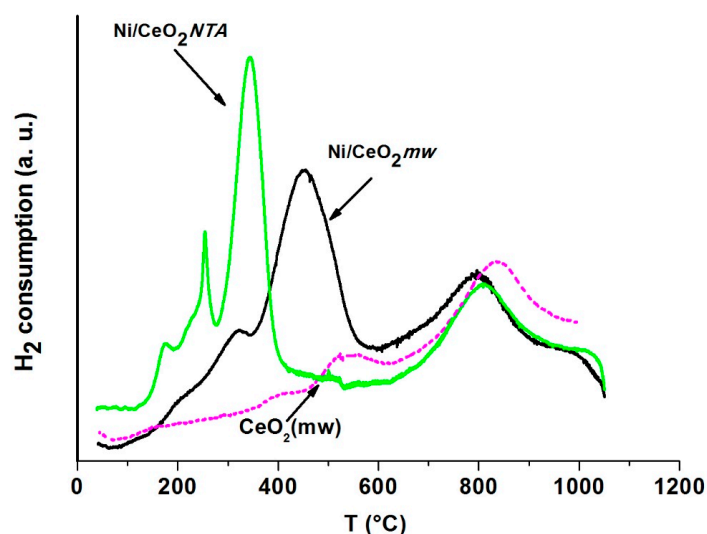
Figure 7. Temperature programmed reduction (TPR) profiles of the two catalysts and the corresponding support CeO_2.

Table 2. T_{max} and H_2 consumption volumes (V) of the TPR peaks that were obtained for the CeO_2 supports and Ni catalysts.

Sample		T_{max} (°C)			V (mL/g_{catal})		
		1st Peak	2nd Peak	3rd Peak	1st Peak	2nd Peak	3rd Peak
Support	CeO_2	-	538	835	-	6	27
Catalyst	Ni/CeO_2*mw*	320	450	796	5	28	27
	Ni/CeO_2*NTA*	250, 170	343	807	6	22	28

The structural effects of the catalytic reaction that was performed on the two samples with and without hydrogen pre-treatment were investigated by X-ray diffraction analyses. The diffraction patterns of the fresh and aged samples are illustrated in Figure 8. All of the patterns contain the fluorite peaks of CeO_2 (ICSD #188051). Moreover, the patterns of the sample that was prepared by microwave co-precipitation, as fresh and aged, do not exhibit any nickel related peaks. On the contrary, the patterns of the sample that was prepared by NTA exhibit NiO (ICSD #9886) related peaks, which become more intense after the CPO reaction, to a large extent in the pre-reduced sample. From the line broadening of the main peaks of CeO_2 and NiO, using the Scherrer equation, the corresponding crystallite sizes were obtained [20]. The values of the fresh and the aged samples after CPO reaction performed with the unreduced and reduced catalysts are summarized in Table 1. The table also lists the lattice parameter of the fluorite structure of CeO_2. According to the table, the value of the CeO_2 lattice parameter did not change upon nickel addition, regardless of the metal introduction procedure.

However, it is worth to say that, if the introduction of Ni into the CeO_2 lattice should cause a decrease of the parameter due to the smaller radius of Ni(II) (0.69 Å), as compared to the Ce(IV) (0.97 Å), at the same time, the consequent generation of new oxygen vacancies would induce a small expansion of the cell. Therefore, the two effects would cancel out and no indication of a real insertion of nickel ions into the ceria lattice can be ascertained [27]. On the bases of the structural characterization, it can be stated that the microwave sample keeps, even after CPO reaction, highly dispersed nickel species, with particle size that is below the XRD detection limit of ~3 nm, and keeps almost constant CeO_2 particle size. On the contrary, the fresh sample that was prepared by NTA complexing agent contains detectable NiO particles of 13 nm, which substantially enlarge after reaction, particularly when the reaction is performed with the pre-reduced sample. Likewise, a significant increase of the CeO_2 particle size occurs.
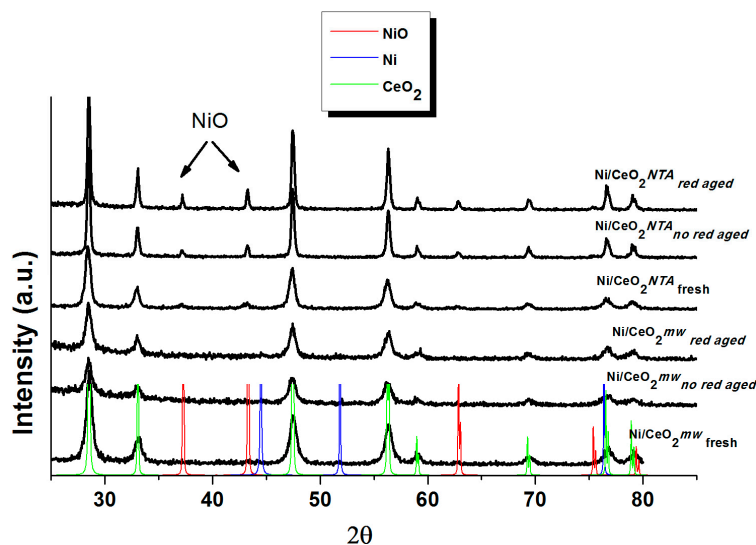
Figure 8. XRD pattern of the two differently prepared samples as fresh and after the CPO cycle performed on the reduced and the un-reduced catalysts.

In accord with the DFT calculation that was reported in the literature, the stronger interaction between nickel and ceria in the microwave sample as compared to the NTA sample, reflected the ability of Ni/CeO$_2$*mw* to activate methane and oxygen, preventing the formation of carbon during CPO reaction [28].

3. Experimental

3.1. Sample Preparation

All of the reagents were from Aldrich and used without further purification. CeO$_2$ support was prepared by precipitation, assisted by microwave. In the synthesis, cerium nitrate hexahydrate was dissolved in ethanol, and then 10 M solution of NaOH was added dropwise until pH = 9. The obtained slurry was placed inside a conventional household microwave and was exposed to the microwaves, according to the previously published procedure [17]. Finally, the collected precipitate was washed, dried at 100 °C for 1h, and then calcined at 550 °C for 2 h. The preparation of the nickel catalysts was achieved by two methods. In one of the methods, the same procedure as the one described above for the ceria support was used, except for adding nickel nitrate and cerium nitrate precursors together. The obtained co-precipitated catalyst is labeled Ni/CeO$_2$*mw*. The second method of nickel loading was carried out by wet-impregnating the prepared CeO$_2$ support with nickel nitrate in the presence of nitrilotriacetic acid (NTA), a tridentate chelating agent [29]. A solution of Ni(NO$_3$)$_2$·6H$_2$O and NTA, previously dissolved in water at pH = 8 was added slowly to the ceria powder, prepared, as described before, and was left impregnating overnight [30]. Then, the solid was dried at 80 °C for 2 h, and thereafter it was calcined at 550 °C. The obtained catalyst was named Ni/CeO$_2$*NTA*. The amount of nickel in both catalysts was 6 wt %, as confirmed by atomic emission spectroscopy.

3.2. Sample Characterization

The specific surface areas of the support and Ni catalysts were determined by N$_2$ physisorption at liquid nitrogen using the Brunauer–Emmett–Teller (BET) method, after sample degassing at 250 °C in high vacuum, as previously described [17]. The obtained BET surface areas are listed in Table 1. It is worth noticing the similarity of the ceria BET area in the pure oxide and in the Ni catalysts.

The phase composition of crystalline components of the fresh and aged samples was investigated by X-ray diffraction (XRD) analyses using a D5000 diffractometer (Bruker AXS, Karlsruhe, Germany),

which was equipped with Cu Kα anode and graphite monochromator [18]. The assignment of the various crystalline phases was based on the Inorganic Crystal Structure Database (ICDS) [31]. An estimation of the mean crystal size values was obtained from the line broadening using the Scherrer equation [20].

Temperature programmed reduction (TPR) experiments were carried out with Autochem 2950 HP apparatus (Micromeritics, Norcross, GA, USA) that was equipped with a thermal conductivity detector (TCD). The gas mixture with composition 5% H_2 in Ar (30 mL/min) was used to reduce the samples (50 mg) heating from room temperature to 1050 °C at the rate of 10 °C/min. Before starting the TPR analyses, the catalysts were pretreated with a flowing gas mixture of 5% O_2 in He (50 mL/min) at 350 °C for 30 min, and then cooling down under He. Using the Micromeritics Autochem provided software (V2.04 A, Autochem II, 2950 HP, Norcross, GA, USA, 2011–2012) the amount of H_2 consumption was estimated by integration of the peak areas after linear baseline substraction.

Thermogravimetric analyses (TGA) of the samples after the catalytic reactions were performed in air using the TGA 1 Star System (Mettler Toledo, Schwerzenbach, Switzerland). About 10 mg of sample were heated from room temperature to 1100 °C at the rate of 10 °C/min. The evolution of the CO_2 was monitored by mass quadrupole.

The X-ray photoelectron spectroscopy (XPS) analyses of the calcined and the spent catalyst powders were performed with a VG Microtech ESCA 3000 Multilab (VG Scientific, Sussex, UK), using Mg Kα source (1253.6 eV) run at 14 kV and 15 mA, and CAE analyser mode [17]. For the individual peak energy regions, a pass energy of 20 eV that was set across the hemispheres was used. The constant charging of the samples was removed by referencing all the energies to the C 1s peak energy set at 285.1 eV, arising from adventitious carbon. Contact of the spent catalysts with air was minimized by keeping them under inert gas until being transferred through a glove box into the XPS instrument. Analyses of the peaks were performed using the CASA XPS software (version 2.3.17, Casa Software Ltd. Wilmslow, Cheshire, UK, 2009). Gaussian (70%)-Lorentzian (30%), defined in Casa XPS as GL(30) profiles were used for each component of the main peaks after a Shirley type baseline subtraction [21]. The binding energy values are quoted with a precision of ±0.15 eV, and the atomic percentage with a precision of ±10%.

3.3. Catalytic Measurements

Methane catalytic partial oxidation tests were performed in a flow system, using a horizontal quartz tube (12 mm inside diameter) with a movable thermocouple for temperature measurements. 100 mg of the catalyst powder (sieved fraction between 180 and 250 μm to avoid intraphase and interphase mass transport [32]) mixed with 200 mg of silicon carbide were placed inside the quartz tube and held with quartz wool on each side of the catalytic bed. Before the reactions, the samples were treated "in situ" under two different conditions. The *no-red* samples were treated with flowing O_2 (5 vol % in He, 50 mL/min) at 350 °C for 1/2 h. The *red* samples, after the O_2 treatment, cooling down to room temperature, were reduced under flowing H_2 (5 vol % in He, 30 mL/min), increasing the temperature to 750 °C with a 10 °C/min ramp and a holding time of 1 h. During this time, two data points for each of the conversion, selectivity, and H_2/CO ratio at a given temperature were registered. The set of values were very close to each other, confirming the steady state condition at a specific temperature. The feed gas consisting of 2 vol % of CH_4 + 1 vol % O_2 in He, was led over the catalyst at a flow rate of 100 mL/min (STP), which was equivalent to a gas hourly space velocity (GHSV) of 60,000 mL g^{-1} h^{-1}. In spite of this relatively high space velocity, the use of a heavily diluted feed and the dilution of the catalyst with inert material minimized overheating of the catalyst bed [2,33]. The activities were measured as a function of temperature from 400 to 800 °C, with a heating rate of 10 °C/min and waiting 60 min for each 50 °C step and back to 600 °C with the same rates. The inlet and outlet gas compositions were analysed by GC (Agilent 7890B, Santa Clara, CA, USA) that was equipped with a DB-1 capillary column and a molecular sieve, in order to follow the evolution of all the species, CH_4, CO, CO_2, H_2, O_2 using flame ionization detector (FID), and TCD detectors. The methane

conversion (X_{CH_4}) and CO and CO_2 selectivities (S_{CO} and S_{CO_2}) were calculated as follows: $X_{CH_4} = 100 \times (CH_4^{in} - CH_4^{out})/CH_4^{in}$; $S_{CO} = 100 \times CO/(CH_4^{in} - CH_4^{out})$; $S_{CO2} = 100 \times CO_2/(CH_4^{in} - CH_4^{out})$. CH_4^{in}, CH_4^{out}, refer to the concentration of methane (ppm) entering and exiting, respectively, the catalytic reactor. CO and CO_2 refer to the concentration (ppm) of CO and CO_2 produced during the reaction. Carbon balance (($CO + CO_2 + CH_{4out})/CH_{4in}$) was 1 ± 0.01 at all temperatures. To investigate the activation of methane by the catalyst surface, temperature-programmed surface reactions (TPSR) were performed using the same sample pretreatment of the CPO reaction, and the same experimental conditions as were used for the TPR reaction, except for the reactant gas being 2 vol % CH_4 in N_2 (CH_4-TPSR reaction). The evolution of CH_4, CO, CO_2, and H_2 was recorded continuously as a function of temperature by using UV and IR ABB detectors.

4. Conclusions

The study has confirmed the importance of the preparation method for CeO_2 supported nickel catalyst, strongly affecting the catalytic performance in methane partial oxidation. The two adopted procedures were successful in the attainment of the two extreme cases, which is typical of the weak and strong metal-support interaction. According to the TPR, XPS, and XRD results, the complexing route using the NTA ligand, allowed for attaining quite small nickel oxide particles, not interacting, freely distributed on the ceria support and easier to reduce. On the contrary, the sample Ni/CeO_2mw, prepared by co-precipitation of nickel and cerium hydroxide assisted by microwaves, contained Ni(II) ions interacting with the support. The interaction was such to enhance the reducibility of the ceria (indeed the TPR bulk ceria reduction peak shifts by about 50 °C and the surface ceria peak by 100 °C to lower temperature), and at the same time, to inhibit the reducibility of the Ni(II) species. In spite of the inhibited reducibility, the catalytic activity of this sample increased and it did not depend on the catalyst pretreatment (oxidative or reductive). On these bases, the presence of metallic nickel before the catalytic reaction was not crucial. The active nickel species likely formed at the first contact with the feed containing the reducing methane. Once the nickel was reduced, the CPO reaction started and the activity continued, being favored by the superior oxygen mobility connected with an increased number of oxygen vacancies that were induced by the nickel in the CeO_2 support. On the contrary, the freshly prepared NTA sample, containing free nickel oxide particles, was active at the beginning of the reaction, when methane starts reducing the nickel and up to a certain temperature. With the increasing reaction temperature, the lack of any interaction with the support produced sintering of the metal particles, quickly deactivating, and reoxidising. In the as reduced state, the catalyst, although being active in CH_4-TPSR, was not able to avoid a quick metal sintering with consequent deactivation.

Author Contributions: A.M.V designed the experiments. V.L.P. performed the materials synthesis, characterization and carried out the catalytic tests. G.P. performed the TPR/TPO and the TGA analyses. A.M.V prepared the manuscript. All three authors contributed to the data discussion and interpretation.

Conflicts of Interest: The authors declare no conflicts of interest.

References

1. Al-Sayari, S.A. Recent developments in the partial oxidation of methane to syngas. *Open Catal. J.* **2013**, *6*, 17–28. [CrossRef]
2. Enger, B.C.; Lødeng, R.; Holmen, A. A review on catalytic partial oxidation of methane to synthesis gas with emphasis on reaction mechanism over transition metal catalysts. *Appl. Catal. A* **2008**, *346*, 1–27. [CrossRef]
3. Wang, Q.; Sun, W.Z.; Jin, G.-Q.; Wang, Y.-Y.; Guo, X.-Y. Biomorphic SiC pellets as catalyst support for partial oxidation of methane to syngas. *Appl. Catal. B* **2008**, *79*, 307–312. [CrossRef]
4. Pengpanich, S.; Meeyo, V.; Rirksomboon, T. Methane partial oxidation over Ni/CeO_2-ZrO_2 mixed oxide solid solution catalyst. *Catal. Today* **2004**, *93–95*, 95–105. [CrossRef]

5. Asencios, Y.J.O.; Nascente, P.A.P.; Assaf, E.M. Partial oxidation of methane on NiO-MgO-ZrO$_2$ catalysts. *Fuel* **2012**, *97*, 630–637. [CrossRef]

6. Zhu, T.; Flytzani-Stephanopoulos, M. Catalytic partial oxidation of metahne to synthesis gas over Ni-CeO$_2$. *Appl. Catal. A* **2001**, *208*, 403–417. [CrossRef]

7. Pal, P.; Singha, R.K.; Saha, A.; Bal, R.; Panda, A.Q.B. Defect-Induced efficient partial oxidation of methane over nonstoichiometric Ni/CeO$_2$ nanocrystals. *J. Phys. Chem. C* **2015**, *119*, 13610–13618. [CrossRef]

8. Nolan, M. Charge transfer and formation of reduced Ce^{3+} upon adsorption of metal atoms at the ceria (110) surface. *J. Chem. Phys.* **2012**, *136*, 134703–134709. [CrossRef] [PubMed]

9. Sayle, D.C.; Sayle, T.C.T. Atomistic modelling of ceria nanostructures: Introducing structural complexity. In *Catalytic Properties of Ceria and CeO$_2$-Containing Materials*, 2nd ed.; Trovarelli, A., Fornasiero, P., Eds.; Imperial College Press: London, UK, 2013; pp. 247–290.

10. Duhamel, L.J.; Zarrou, H.; D'Huysser, A. Hydrogen production at low temperature from methane on cerium and nickel based mixed oxide. *Int. J. Hydrogen Energy* **2008**, *33*, 5527–5534.

11. Zou, W.; Ge, C.; Lu, M.; Wu, S.; Wang, T.; Sun, J.; Pu, Y.; Tang, C.; Gao, F.; Domg, L. Engineering the NiO/CeO$_2$ interface to enhance the catalytic performance for CO oxidation. *RSC Adv.* **2015**, *5*, 98335–98341. [CrossRef]

12. Zhang, X.; You, R.; Li, D.; Cao, T.; Huang, W. Reaction sensitivity of ceria morphology effect on Ni/CeO$_2$ catalysis in propane oxidation reactions. *Appl. Mater. Interface* **2017**, *9*, 35897–35907. [CrossRef] [PubMed]

13. Moraes, T.S.; Neto, R.C.R.; Ribeiro, M.C.; Mattos, L.V.; Kourtelesis, M.; Verykios, X.; Noronha, F.B. Effects of ceria morphology on catalytic performances of Ni/CeO$_2$ Catalysts for low temperature steam reforming of ethanol. *Top. Catal.* **2015**, *58*, 281–294. [CrossRef]

14. Jin, R.; Chen, Y.; Li, W.; Cui, W.; Ji, Y.; Yu, C.; Jiang, Y. Mechanism for catalytic partial oxidation of methane to syngas over a Ni/Al$_2$O$_3$ catalyst. *Appl. Catal. A* **2000**, *201*, 71–80. [CrossRef]

15. Shan, W.; Fleys, M.; Lapicque, F.; Swierczynski, D.; Kiennemann, A.; Simon, Y.; Marquaire, P.-M. Syngas production from partial oxidation of methane over Ce$_{1-X}$Ni$_X$O$_Y$ catalysts prepared by complexation-combustion method. *Appl. Catal. A* **2006**, *311*, 24–33. [CrossRef]

16. Singha, R.K.; Shukla, A.; Yadav, A.; Konathala, L.N.S.; Bal, R. Effect of metal-support interaction on activity and stability of Ni-CeO$_2$ catalyst for partial oxidation of methane. *Appl. Catal. B* **2017**, *201*, 473–488. [CrossRef]

17. Pantaleo, G.; la Parola, V.; Deganello, F.; Singha, R.K.; Bal, R.; Venezia, A.M. Ni/CeO$_2$ catalysts for methane partial oxidation: Synthesis driven structural and catalytic effects. *Appl. Catal. B* **2016**, *189*, 233–241. [CrossRef]

18. Pantaleo, G.; la Parola, V.; Deganello, F.; Calatozzo, P.; Bal, R.; Venezia, A.M. Synthesis and support composition effects on CH$_4$ partial oxidation over Ni-CeLa oxides. *Appl. Catal. B* **2015**, *164*, 135–141. [CrossRef]

19. Li, Y.; Zhang, B.; Tang, X.; Xu, Y.; Shen, W. Hydrogen production from methane decomposition over Ni/CeO$_2$ catalysts. *Catal. Commun.* **2006**, *7*, 380–386. [CrossRef]

20. Klug, H.P.; Alexander, L.E. *X-ray Diffraction Procedures for Polycrystalline and Amorphous Materials*, 2nd ed.; John Wiley and Sons: New York, NY, USA, 1974.

21. Biesinger, M.C.; Payen, B.P.; Lau, L.W.M.; Gerson, A.; Smart, R.S.C. X-ray photoelectron spectroscopic chemical state quantification of mixed nickel metal, oxide and hydroxide systems. *Surf. Interface Anal.* **2009**, *41*, 324–332. [CrossRef]

22. Renuka, N.K.; Harsha, N.; Divya, T. Supercharged ceria quantum dots with exceptionally high oxygen buffer action. *RSC Adv.* **2015**, *5*, 38837–38841. [CrossRef]

23. Răduțoiu, N.; Teodorescu, C.M. Satellites in Ce 3d X-ray photoelectron spectroscopy of ceria. *Dig. J. Nanomater. Biostruct.* **2013**, *8*, 1535–1549.

24. Choudhury, B.; Choudhury, A. Ce^{3+} and oxygen vacancy mediated tuning of structural and optical properties of CeO$_2$ nanoparticles. *Mater. Chem. Phys.* **2012**, *131*, 666–671. [CrossRef]

25. Paparazzo, E.; Ingo, G.M.; Zacchetti, N. X-ray induced reduction effects at CeO$_2$ surfaces: An X-ray photoelectron spectroscopy study. *J. Vac. Sci. Technol. A* **1991**, *9*, 1416–1419. [CrossRef]

26. Diskin, A.M.; Cunningham, R.H.; Ormerod, R.M. The oxidative chemistry of methane over supported nickel catalysts. *Catal. Today* **1998**, *46*, 147–154. [CrossRef]

27. Qin, W.; Xie, K.; Liu, M.; Wiu, G.; Wang, Y.; Zhang, Y. Single phase nickel-doped ceria cathode with in situ grown nickel nanocatalyst for direct high temperature carbon dioxide electrolysis. *RSC Adv.* **2014**, *4*, 40494–40504.

28. Liu, Z.; Grinter, D.C.; Lustemberg, P.G.; Nguyen-Phan, T.; Zhou, Y.; Luo, S.; Waluyo, I.; Crumlin, E.J.; Stacchiola, D.J.; Zhou, J.; et al. Dry reforming of methane on a highly active Ni-CeO$_2$ catalyst: Effects of metal-support interactions on C-H bond breaking. *Angew. Chem. Int. Ed. Engl.* **2016**, *55*, 7455–7459. [CrossRef] [PubMed]

29. Van Dillen, A.J.; Terorde, R.J.A.M.; Lensveld, D.J.; Geus, J.W.; de Jong, K.P. Synthesis of supported catalysts by impregnation and drying using aqueous chelated metal complexes. *J. Catal.* **2003**, *216*, 257–264. [CrossRef]

30. Venezia, A.M.; la Parola, V.; Deganello, G.; Cauzzi, D.; Leonardi, G.; Predieri, G. Influence of the prepration method on the thiophene HDS activbity of silica supported CoMo catalysts. *Appl. Catal. A* **2002**, *229*, 261–271. [CrossRef]

31. Inorganic Crystal Structure Database (ICSD). *Fachinformationszentrum Karlsruhe*; Inorganic Crystal Structure Database: Karlsruhe, Germany, 2014.

32. Lødeng, R.; Bjørgum, E.; Enger, B.C.; Eilertsen, J.L.; Holmen, A.; Krogh, B.; Rønnekleiv, M.; Rytter, E. Catalytic partial oxidation of CH$_4$ to H$_2$ over cobalt catalysts at moderate temperatures. *Appl. Catal. A* **2007**, *333*, 11–23. [CrossRef]

33. Boucouvalas, Y.; Zhang, Z.; Verykios, X.E. Heat transport limitations and reaction scheme of partial oxidation of methane to synthesis gas over rhodium catalysts. *Catal. Lett.* **1994**, *27*, 131–142. [CrossRef]